RSC Advances

PAPER

View Article Online
View Journal | View Issue

Cite this: *RSC Adv.*, 2020, **10**, 12780

Effect of lignite as support precursor on deep desulfurization performance of semicoke supported zinc oxide sorbent in hot coal gas

Ting Li, Xiurong Ren,* Liuxu Bao, Meijun Wang, Weiren Bao and Liping Chang*

In this study, four different semicoke supported zinc oxide sorbents were prepared by combining high-pressure impregnation and heat treatment using four different lignites (Zhaotong, Xiaolongtan, Huolinhe, and Shengli districts) as precursors of supports and zinc nitrate as precursor of the active component. Their desulfurization performances were studied in a fixed-bed reactor at 400 °C in simulated coal gas. The physico-chemical properties of raw lignites were investigated using chemical titration, nitrogen adsorption and thermogravimetry (TG). The physico-chemical structures of sorbents were characterized by atomic absorption spectrometry (AAS), X-ray diffraction analysis (XRD), nitrogen adsorption, and scanning electron microscopy (SEM). The results indicate that the lignite as support precursor plays a critical role in the desulfurization performance of the sorbent. It affects the desulfurization activity of the prepared sorbent by influencing the loading content and utilization rate of the active component of the sorbent. The sorbent HPZn/C(Z) prepared using Zhaotong lignite presents the best desulfurization performance owing to its higher content and utilization rate of the active component, with a 13.74 h breakthrough time with the breakthrough sulfur capacity of 3.69 g sulfur/100 g sorbent. It is found that the loading content of the active component depends on the pore structure of the raw lignite, how its pore structure changes in high-pressure impregnation process and the content of oxygen-containing functional groups on its surface. The utilization rate of the active component is associated with the pore structure properties of the sorbent formed during heat treatment.

Received 24th December 2019
Accepted 18th March 2020

DOI: 10.1039/c9ra10884j

rsc.li/rsc-advances

1. Introduction

The clean coal technologies are critical to improve energy utilization efficiency and reduce the pollution of the environment for some countries who depend on coals as the main source of energy.[1] Gasification is a very efficient method in clean coal technologies. In the process, approximately 80% of the sulfur in coal will be transformed into sulfur gases such as H_2S, COS and CS_2, of which H_2S accounts for about 90%. The presence of H_2S in coal gas could lead to serious equipment corrosion and catalyst poisoning in downstream processes.[2,3] The total sulfur content of coal gas need to be reduced to less than 100 ppm for IGCC, 1 ppm for fuel cell or 0.1–1 ppm for chemical production.[4] Therefore, the hydrogen sulfide has to be removed before downstream processes.

H_2S removal using metal oxide sorbents at high temperature is a significant desulfurization technology. It can not only improve thermal efficiency, but also reduce equipment cost without gas cooling and reheating processes compared with the conventional wet desulfurization. So far, various single and mixed metal oxide sorbents prepared by different methods were studied for hot coal gas desulfurization,[5–19] such as oxides of iron, manganese, zinc, copper, cerium, calcium, and cobalt. In view of deep desulfurization, zinc oxide is regarded as the most attractive candidate sorbent owing to its high precision and good thermal stability for H_2S removal.[20] In addition, various porous materials, which are used as supports to improve the properties of sorbents, were also investigated. The porous supports mainly contain γ-Al_2O_3, mesoporous silica, zeolite, and carbon materials.[21–27] Carbon materials including activated carbon and semicoke have attracted more and more researchers' attention due to their abundant pore structure and low cost. In comparison with activated carbon, semicoke is cheaper and more easily attained. Lignite has larger porosity and higher pyrolysis reactivity compared with other coals, making it a good raw material for semicoke preparation. In addition, lignite has higher water absorption ability, which is beneficial for loading active component on its surface by impregnation method.

In consideration of these, our group proposed to prepare a semicoke supported zinc oxide sorbent for deep desulfurization by combining impregnation and heat treatment using lignite as precursor of support and zinc nitrate as precursor of active component. The advantage of this method is that the

Key Laboratory of Coal Science and Technology, Taiyuan University of Technology, Ministry of Education and Shanxi Province, Taiyuan 030024, PR China. E-mail: renxiurong@tyut.edu.cn; lpchang@tyut.edu.cn

preparation of semicoke and the decomposition of active component precursor are accomplished simultaneously during heat treatment, simplifying preparation process of sorbents. In our previous studies, different impregnation methods were investigated. The results show that the sorbents obtained by high-pressure impregnation and heat treatment method have good desulfurization performance. It is because high-pressure impregnation can improve the pore structure of the lignite compared with other impregnation methods and make more active components loading on its surface.[28] The conditions of high-pressure impregnation and heat treatment were also optimized.[29,30] Lignite, as the precursor of support, could have significant effect on the desulfurization performance of sorbent prepared by this method. So, the effect of different lignites as precursor of support on desulfurization performance of the sorbents should be investigated. In China, lignite resources are mainly distributed in Inner Mongolia and Yunnan province. Due to different coal-forming periods, the lignites from Yunnan province belong to young lignite and those from Inner Mongolia belong to old lignite. The physico-chemical properties of young lignite and old lignite are different. Therefore, in this paper, two young lignites from Zhaotong and Xiaolongtan districts of Yunnan and two old lignites from Huolinhe and Shengli districts of Inner Mongolia were selected as the precursor of support to prepare semicoke supported zinc oxide sorbents by aforementioned method. The effects of these lignites on the performances and desulfurization activities of the sorbents were investigated.

2. Experimental section

2.1 Sorbent preparation

The lignites from Zhaotong, Xiaolongtan, Huolinhe and Shengli districts were named as ZT, XLT, HLH and SL. The proximate and ultimate analyses of the lignites are shown in Table 1. The preparation procedures of sorbent are as follows. The lignite was crushed and sieved to the particle size range of 2.36–3.35 mm (6–8 mesh), and then was dried at 80 °C in vacuum oven for 4 h. The dry lignites were named as R/C(Z), R/C(X), R/C(H) and R/C(S), where R represents the raw coal and Z, X, H and S represent ZT, XLT, HLH and SL, respectively. The dry lignite (20 g) was attached to $Zn(NO_3)_2$ solution (36 wt%, 34 mL) in sealed autoclave and heated at 213 °C (corresponding to 20 atm in sealed autoclave) for 5 h in muffle furnace. Then, the autoclave was cooled down to room temperature, and the sample was filtered and dried at 80 °C in vacuum oven for 6 h. The impregnated lignites were named as PZn/C(Z), PZn/C(X), PZn/C(H) and PZn/C(S), where PZn represents high-pressure impregnation in $Zn(NO_3)_2$ solution. Finally, the sample was placed in a fixed-bed quartz reactor (internal diameter 20 mm) and heated in N_2 atmosphere (500 mL min^{-1}) from room temperature to 550 °C at a heating rate of 10 °C min^{-1} and maintained at 550 °C for 3 h. The prepared sorbents were named as HPZn/C(Z), HPZn/C(X), HPZn/C(H) and HPZn/C(S) where H represents the heat treatment. For comparison purpose, four corresponding lignite semicokes were also prepared according to the above method and condition only with $Zn(NO_3)_2$ solution replaced by deionized water. The prepared lignite semicokes were named as HPW/C(Z), HPW/C(X), HPW/C(H) and HPW/C(S).

Table 1 Proximate and ultimate analyses of lignites

	Sample			
Items	ZT	XLT	HLH	SL
Proximate (wt%)				
Moisture (ad)	16.74	19.45	13.55	14.39
Volatile (daf)	53.08	59.76	50.00	49.12
Ash (d)	16.24	8.17	3.98	7.34
Ultimate (wt%, daf)				
Carbon	65.94	69.62	74.91	74.88
Hydrogen	4.63	4.10	4.65	4.22
Oxygen	27.19	23.20	18.21	19.01
Nitrogen	1.54	1.96	1.09	0.87
Sulfur	0.70	1.12	1.14	1.02

2.2 Desulfurization test

The desulfurization tests were implemented in a fixed-bed quartz reactor (inner diameter of 20 mm) with an external heating furnace, as shown in Fig. 1. Approximate 13 g (20 mL) sorbent was used for each experiment. All desulfurization experiment were conducted at 400 °C under 2000 h^{-1} space velocity with atmosphere pressure. The inlet gas was simulated coal gas, composed of CO (33%), H_2 (39%), CO_2 (19.7%), H_2O (1%), H_2S (500 ppm) and N_2 (balance) by volume fraction. The H_2S concentration in the gas was detected by a gas chromatograph (GC950, Shanghai Haixin) with a flame photometry detector.

H_2S breakthrough time, breakthrough sulfur capacity and utilization rate of active component were used to evaluate the desulfurization performance of sorbent. When the outlet concentration of H_2S reached 1 ppm, the sorbent bed was regarded as breakthrough. The breakthrough time was designated as the time from the beginning of experiment to the breakthrough of sorbent bed. The breakthrough sulfur capacity was the weight of sulfur adsorbed by 100 g sorbent in the breakthrough time, which was calculated using the following equation:

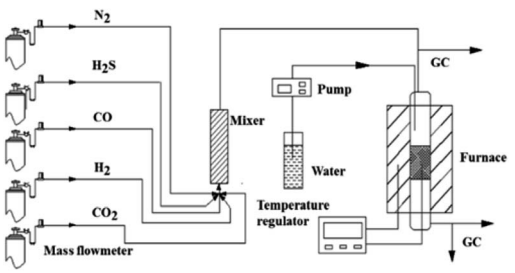

Fig. 1 Schematic diagram of experimental device.

$$S_b(\text{g sulfur}/100\text{ g sorbent}) = \sum \frac{32\nu_{sp}V_s}{22.4W_s}\int_0^{t_b}(C_{in}-C_{out})dt \quad (1)$$

where S_b is the breakthrough sulfur capacity; ν_{sp} is space velocity of inlet gas, h^{-1}; V_s is the volume of the sorbent, L; W_s is the weight of sorbent, g; C_{in} and C_{out} are H_2S concentration in the inlet and outlet gases respectively, ppm; t_b is H_2S breakthrough time, h.

The calculation equation of utilization rate of active component (Zn) was as follows:

$$Y(\%) = \frac{S_b}{S_t}\times 100 \quad (2)$$

where Y is utilization rate of active component; S_b is breakthrough sulfur capacity; S_t is theoretical sulfur capacity, *i.e.* the mass adsorbed by 100 g sorbent assuming that the active component of sorbent reacts completely with H_2S.

The desulfurization tests were carried out twice for each sorbent, the average value and standard deviation of H_2S breakthrough time and breakthrough sulfur capacity were calculated.

2.3 Sorbent characterization

The crystal structures of the sorbents were recorded by an X-ray diffractometer (Rigaku, D/max-2500, Japan) with Cu Kα radiation at 30 mA and 40 kV respectively. The diffraction patterns were recorded from 5° to 80° at a scanning speed of 8° min^{-1}.

The metal contents in the samples were analyzed by an atomic absorption spectrum instrument (AA240FS, America) with working lamp current of 2.0 mA.

The content of oxygen-containing functional groups including phenolic hydroxyl (Ar-OH) and carboxyl (COOH) groups were quantitatively analyzed with chemical titration and ion exchange method. The detailed procedure can be found in previous literature.[31]

The measures of the metal contents and oxygen-containing functional groups contents of the samples were also repeated for another time. The average value and standard deviation for the data were calculated.

The pore structures of the samples were measured using the nitrogen adsorption analyzer (JW-BK122W, JWGB, China). The specific surface area (S_{total}) of samples was measured by Brunauer–Emmet–Teller (BET) equation. The micro-pore volume (V_{micro}) and micro-pore surface area ($S_{internal}$) were assessed according to *t*-plot model. The meso-pore volume (V_{meso}) was calculated according to Barret–Joyner–Halenda (BJH) model. The external surface area ($S_{external}$) was obtained by difference of S_{total} and $S_{internal}$. The total pore volume (V_{total}) was the sum of V_{micro} and V_{meso}.

The pyrolysis characteristics of raw lignites were investigated *via* a thermogravimetric analyzer (STA449F3, NETZSCH, Germany). The pyrolysis was carried out from room temperature to 900 °C at a heating rate of 10 °C min^{-1} in ambient pressure with 100 mL min^{-1} nitrogen. 30 mg coal sample was used for each experiment.

The surface morphologies of the sorbents were obtained by scanning electron microscope (TESCAN MAIA 3 LMH, Czech Republic). The scanning voltage is 20.0 kV.

3. Results and discussion

3.1 Desulfurization performance of sorbents

The sulfidation breakthrough curves and breakthrough sulfur capacities of the lignite semicokes and the sorbents are shown in Fig. 2. The sorbents exhibited significantly different desulfurization performance. The order of desulfurization activities of four sorbents are HPZn/C(Z) > HPZn/C(S) > HPZn/C(H) > HPZn/C(X). The breakthrough time of the HPZn/C(Z) was 13.74 h and the corresponding breakthrough sulfur capacity can reach 3.69 g sulfur/100 g sorbent. However, the breakthrough time and breakthrough sulfur capacity of the HPZn/C(X) were only 1.08 h and 0.29 g sulfur/100 g sorbent respectively. It shows that the lignites as precursors of supports have a great influence on the desulfurization performance of sorbents. It can also be observed that the lignite semicokes had hardly desulfurization capability, suggesting the ashes in the semicokes were inert and desulfurization performance of the sorbents mainly depended on their active components. In addition, it is noted that these sorbents had very high precision of desulfurization, no H_2S detected in outlet gas before breakthrough, owing to larger reaction equilibrium constant of active component.

3.2 Characterization of sorbents

In order to reveal the significant difference of desulfurization performance of the sorbents, the physico-chemical properties of raw lignites, impregnated lignites and sorbents were investigated by relevant characterization techniques. The XRD patterns of the fresh and sulfided sorbents are displayed in Fig. 3. From Fig. 3(a), the wurtzite crystalline phase of ZnO diffraction peaks were observed for all sorbents, showing the

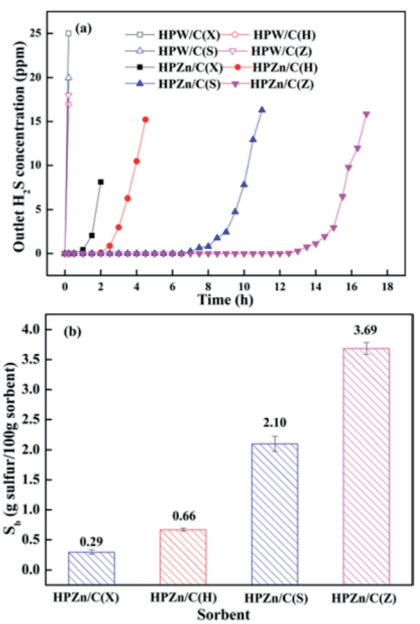

Fig. 2 Desulfurization curves (a) and breakthrough sulfur capacities (b) of sorbents.

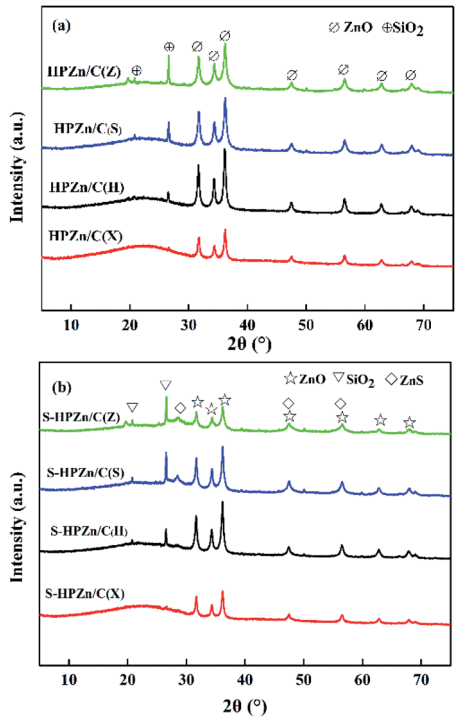

Fig. 3 XRD patterns of the fresh (a) and sulfided sorbents (b).

Table 2 Zn loading contents of the impregnated lignites

Sample	PZn/C(X)	PZn/C(H)	PZn/C(S)	PZn/C(Z)
Zn content (%)	9.20 ± 0.13	18.71 ± 0.11	17.73 ± 0.18	18.38 ± 0.22

same kind of ZnO for these sorbents. But the peak intensities of ZnO were different, mainly due to the difference of Zn contents in sorbents. Apparently, the intensities of ZnO diffraction peaks were generally consistent with the Zn loading contents in the sorbents shown in Table 3. In addition, SiO_2 diffraction peaks were also found in the sorbents except for HPZn/C(X). SiO_2 is mineral in lignite, and it remains in semicoke after heat treatment. No SiO_2 diffraction peaks were observed in HPZn/C(X) probably due to low SiO_2 content in semicoke. The broad humps were attributed to microcrystalline graphite carbon. From Fig. 3(b), the diffraction peaks of ZnS were observed in the sorbents after desulfurization, confirming that ZnO was converted into ZnS through the reaction $ZnO + H_2S \rightarrow ZnS + H_2O$.

Zn loading contents of the impregnated lignites and sorbents were measured by an atomic absorption spectrum, and Zn utilization rates of the sorbents were calculated through the breakthrough sulfur capacity and theoretical sulfur capacity. The results are shown in Tables 2 and 3. It can be seen that Zn loading contents of the impregnated lignites were no significant difference except for the PZn/C(X). Zn loading contents of the PZn/C(H), PZn/C(S), and PZn/C(Z) were in the range of 17.73–18.71% while that of the PZn/C(X) was only 9.20%. After heat treatment, Zn loading contents of the sorbents decreased by approximate 3–5% compared with corresponding impregnated lignites, due to pyrolysis of the lignites and decomposition of zinc nitrate in heat treatment process. As a result, the Zn loading contents of the HPZn/C(H), HPZn/C(Z), and HPZn/C(S) were in the range of 13.33–14.06% while that of the HPZn/C(X) was only 6.40%. The difference of Zn utilization rates of the sorbents was greater. They varied from 9.28% to 53.95%. Combined with the breakthrough sulfur capacity of the sorbents, it can be found that the breakthrough sulfur capacity of the HPZn/C(X) was only 0.29 g due to its lowest Zn loading content and utilization rate (6.40% and 9.28%). The breakthrough sulfur capacity of the HPZn/C(H) was only 0.66 g S/100 g sorbent, although its Zn loading content was the highest in all sorbents and slightly higher that of the HPZn/C(X). Compared with the theoretical sulfur capacity, the utilization rate of Zn for HPZn/C(H) is only 9.67%. The similar phenomenon was observed for sorbent HPZn/C(S). Sorbent HPZn/C(Z) with higher Zn content and the highest utilization rate of Zn has the highest sulfur capacity. Apparently, the lignite as support precursor affected the desulfurization activity of the sorbent by influencing content and utilization rate of active component. The higher content and utilization rate of Zn are indispensable for good desulfurization performance of sorbent.

In order to further understand the causes that lead to the difference of Zn loading contents in sorbents, pore structures of raw lignites and impregnated lignites were characterized by nitrogen adsorption analyzer. Generally, higher pore volume and specific surface area are beneficial to adsorbing ions of active component in solution. As displayed in Fig. 4, the pore volume and specific surface area of the R/C(H) was obviously higher than those of other raw lignites. After high pressure impregnation, the pore volumes and specific surface areas of raw lignites increased to some degree. The increases of pore volumes and specific surface areas of the PZn/C(S) and PZn/C(Z) were more evident in comparison with corresponding raw lignites. It indicates that high pressure impregnation can improve pore volume and specific surface area of raw lignite, which is advantageous for adsorption of zinc ion in solution. That is because in high-pressure impregnation process, the liquid has stronger ability of penetrating and dissolving matter.[30] The hot solution can open some blocked pores of raw

Table 3 Loading contents and utilization rates of Zn

Sorbent	Zn content (%)	S_b (g S/100 g sorbent)	S_t (g S/100 g sorbent)	Zn utilization rate (%)
HPZn/C(X)	6.40 ± 0.15	0.29 ± 0.04	3.15 ± 0.07	9.28 ± 0.91
HPZn/C(H)	14.06 ± 0.08	0.66 ± 0.03	6.92 ± 0.04	9.67 ± 0.44
HPZn/C(S)	13.33 ± 0.10	2.10 ± 0.12	6.56 ± 0.05	32.01 ± 2.0
HPZn/C(Z)	13.88 ± 0.11	3.69 ± 0.10	6.83 ± 0.05	53.95 ± 1.05

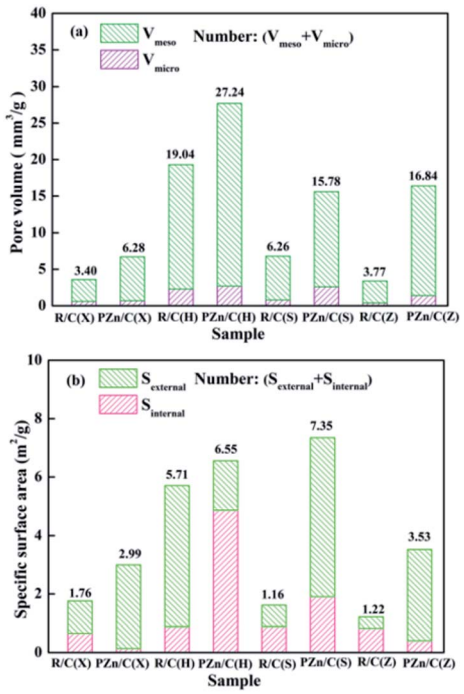

Fig. 4 Pore structures of raw lignites and impregnated lignites ((a) pore volume, (b) specific surface area).

lignite and dissolve some minerals in pore wall, resulting in increase of pore volume and specific surface area.

Combined with Zn loading content of the impregnated lignites in Table 2, it can be found that Zn loading contents of the impregnated lignites were associated with their pore volumes and specific surface areas. Zn loading content of the PZn/C(X) was only 9.20%, because of its smaller V_{tot} and S_{tot} (6.28 $mm^3\ g^{-1}$ and 2.99 $m^2\ g^{-1}$). The PZn/C(H) with larger V_{tot} and S_{tot} (27.24 $mm^3\ g^{-1}$ and 6.55 $m^2\ g^{-1}$) had higher Zn loading content (18.71%). It is also noted that Zn loading content of the PZn/C(Z) was close to that of the PZn/C(H), although both of its pore volume and specific surface area were smaller than those of the PZn/C(H). It indicates that factors determining Zn loading are not limited to pore volume and specific surface area.

The surface of lignite is rich in oxygen-containing groups such as carboxyl and phenolic hydroxyl groups, which can act as cation-exchange site.[32,33] The zinc ion could be loaded on the lignite by ion exchange. Therefore, oxygen-containing groups of raw lignite may be another factor affecting Zn loading content. The oxygen-containing functional groups contents of raw lignites are shown in Fig. 5. It is found that the R/C(Z) had higher oxygen-containing groups content compared with other raw lignites, which favored Zn loading. Therefore, although pore volume and specific surface area of the PZn/C(Z) were smaller than those of the PZn/C(H), Zn loading content of the PZn/C(Z) was similar to that of the PZn/C(H).

In order to further explore the reasons that affect Zn utilization rates of the sorbents, pore structures of the sorbents were characterized, as displayed in Fig. 6. Combining Zn utilization

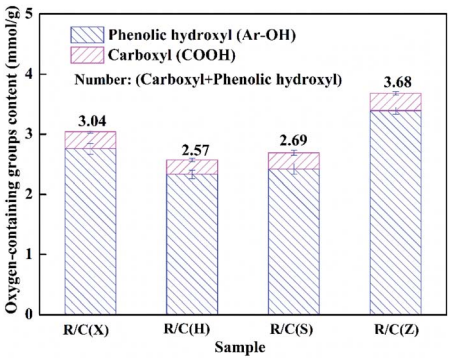

Fig. 5 Oxygen-containing groups content of raw lignites.

rates of the sorbents mentioned in Table 3, it is found that Zn utilization rate (9.67%) of the HPZn/C(H) with the highest S_{tot} and V_{tot} was smaller than those of HPZn/C(S) and HPZn/C(Z) (32.01% and 53.95%). It is noted that the HPZn/C(H) have smaller $S_{external}/S_{total}$ and V_{meso}/V_{total} compared with HPZn/C(S) and HPZn/C(Z). It can be inferred that $S_{external}/S_{total}$ and V_{meso}/V_{total} are significant factors that influence Zn utilization rate. Because the sulfidation of metallic oxide is a gas–solid reaction, during which oxygen atom of ZnO is substituted by the larger sulfur atom and the product ZnS takes up more space than the reactant ZnO. The micropore will be easily blocked in the course of reaction. This means that the diffusion resistance will become more and more severe and sulfidation will become more and more difficult, as reaction progresses.[7] Therefore, the

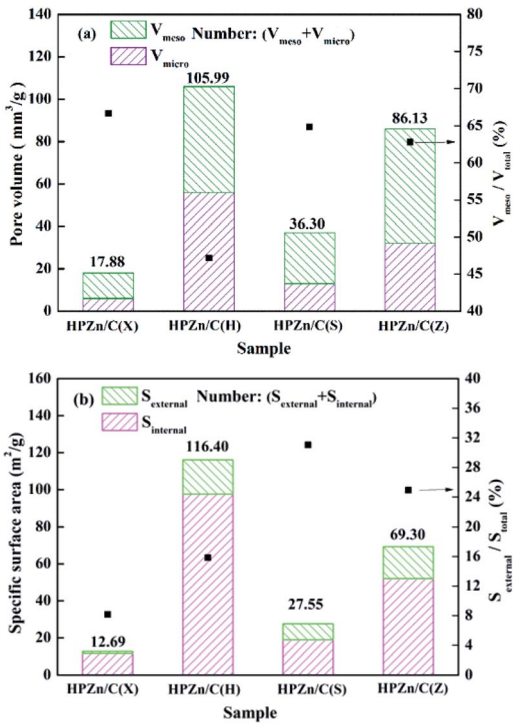

Fig. 6 Pore structures of the sorbents ((a) pore volume, (b) specific surface area).

active component on the external surface is more effective than that on the internal surface. Therefore, although the S_{tot} and V_{tot} of the HPZn/C(H) (116.40 m^2 g^{-1} and 105.99 mm^3 g^{-1}) were higher than those of the HPZn/C(S) (27.55 m^2 g^{-1} and 36.30 mm^3 g^{-1}), its Zn utilization (9.67%) was lower than that of the HPZn/C(S) (32.01%). It is attributed to the $S_{external}/S_{total}$ and V_{meso}/V_{total} of the HPZn/C(H) (15.84% and 47.16%) were smaller than those of the HPZn/C(S) (31.04% and 64.84%). Comparing the HPZn/C(S) and HPZn/C(Z), the Zn utilization rate (53.95%) of the HPZn/C(Z) was higher than that of the HPZn/C(S) (32.01%), although their $S_{external}/S_{total}$ and V_{meso}/V_{total} were close. It is observed that S_{total} and V_{total} of the HPZn/C(Z) (69.30 m^2 g^{-1} and 86.13 mm^3 g^{-1}) were higher than the HPZn/C(S) (27.55 m^2 g^{-1} and 36.30 mm^3 g^{-1}). Because the larger S_{total} and V_{total} are favorable for the dispersion of active component on the support, which make active component more reactive. Overall, the combination of S_{total}, V_{total} and $S_{external}/S_{total}$, V_{meso}/V_{total} determines utilization rate of active component. The larger $S_{external}/S_{total}$ and V_{meso}/V_{total} of the sorbent are favorable for Zn effective utilization. Meanwhile, the larger S_{total} and V_{total} of the sorbent are also beneficial for Zn effective utilization when its $S_{external}/S_{total}$ and V_{meso}/V_{total} are larger.

The pore structures of the sorbents were reconstituted during heat treatment. Therefore, the pore structures of the sorbents were related with pyrolysis characteristics of raw lignites. The pyrolysis characteristics of raw lignites were investigated by thermogravimetric analysis. TG/DTG curves of raw lignites are presented in Fig. 7. From Fig. 7(b), it can be seen that the first weight loss peak in the temperature below 200 °C was observed,

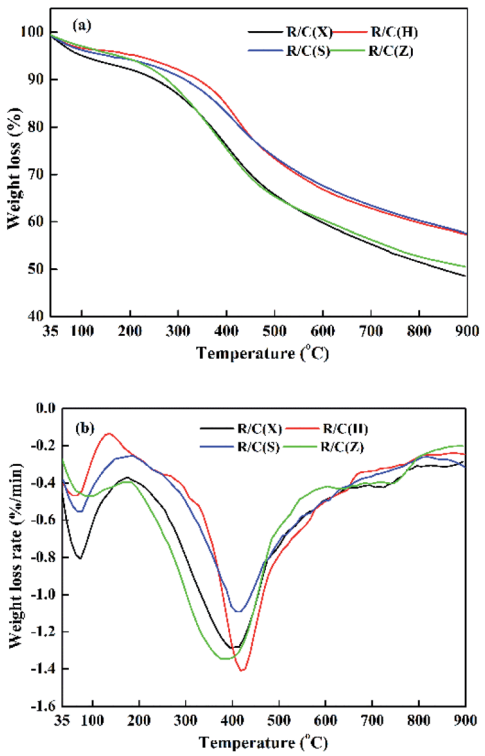

Fig. 7 TG/DTG curves of raw lignites ((a) weight loss, (b) weight loss rate).

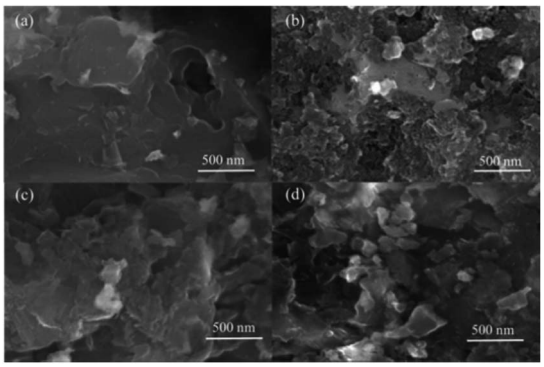

Fig. 8 SEM images of sorbents ((a) HPZn/C(X), (b) HPZn/C(H), (c) HPZn/C(S), (d) HPZn/C(Z)).

which was attributed to the removal of water and adsorbed gases from lignite. A broad weight loss peak was observed between around 200 °C and 600 °C, which was due to the release of lots of volatiles in the main pyrolysis stage. When the temperature was over 600 °C, a slight weight loss peak was found, which was because of decomposition of carbonates in lignite to generate CO_2 and the condensations of aromatic rings to release H_2. In the temperature range of 200–600 °C, the peak temperatures of the R/C(Z) and R/C(X) were lower than those of the R/C(S) and R/C(H), suggesting R/C(Z) and R/C(X) are lower rank coal compared with the R/C(S) and R/C(H). In general, a lower rank coal loses more weight during pyrolysis in comparison to a higher rank coal. And the peak size of the R/C(Z) and R/C(H) were greater than the R/C(X) and R/C(S) respectively, indicating the R/C(Z) and R/C(H) could release more volatiles fastly compared with the R/C(X) and R/C(S) in the temperature range of 200–600 °C. This may be one of the reasons that the S_{tot} and V_{tot} of HPZn/C(Z) and HPZn/C(H) were higher among the sorbents. Because during pyrolysis process, the pore structure of lignite can be promoted dramatically, which is mainly attributed to change of matrix structure caused by sharp release of volatile. However due to the complexity of coal, we can't reveal the difference of $S_{external}/S_{total}$ and V_{meso}/V_{total} for these sorbents from the TG/DTG curves.

The surface morphologies of the sorbents were also observed by SEM. The images are illustrated in Fig. 8. From Fig. 8, the morphologies of sorbents were significantly different. The surface of the HPZn/C(X) was much smoother with less porosity compared with other sorbents which had porous structure. The pores of the HPZn/C(H) seemed more abundant than those of the HPZn/C(S) and HPZn/C(Z). It was consistent with the results of pore structures of sorbents (in Fig. 6) that the HPZn/C(H) had the largest S_{total} and V_{total} among the sorbents. Some white dots could be found in the images, which were the ZnO active component particles.[20] The ZnO particles on the surface of the HPZn/C(X) was less due to its low loading content of active component.

3.3 Comparison of HPZn/C(Z) and other sorbents in literatures

The desulfurization performance of the most active sorbent (HPZn/C(Z)) found in this work and other sorbents in the

Table 4 Desulfurization performance of HPZn/C(Z) and other sorbents in the literature[a]

Sorbent	Zn Loading content (%)	S_b (g S/100 g sorbent)	Zn utilization rate (%)	Ref.
HPZn/C(Z)	13.88	3.69	53.95	
ZnO/SC	23.82[b]	4.46	38	35
I-ZnO/AC	—	1.58	—	34
II-ZnO/AC	27.82[b]	4.52	33	35
I-ZnO/γ-Al_2O_3	5	0.65	26.42[b]	36
II-ZnO/γ-Al_2O_3	15.12[b]	2.01	27	35
ZnO/4A	29.32[b]	3.32	23	35
ZnO/SBA-15	—	0.9–1.8	—	37

[a] SC: semicoke, AC: activated carbon, 4A: 4A molecular sieve, SBA15: SBA-15 molecular sieve. [b] Calculation by data in the literature.

literature was shown in Table 4. Among the sorbents, the HPZn/C(Z), ZnO/SC and II-ZnO/AC exhibited good desulfurization performance with higher breakthrough sulfur capacity and Zn utilization rate. Compared with the II-ZnO/AC, even though Zn loading content of the HPZn/C(Z) was only about fifty percent of the II-ZnO/AC, its breakthrough sulfur capacity was about eighty percent of the II-ZnO/AC. It was attributed to the higher Zn utilization rate of the HPZn/C(Z).

4. Conclusions

In this paper, four different lignites were chosen as precursor of support to prepare semicoke supported zinc oxide sorbents, and the effects of these lignites on the desulfurization performances of sorbents were investigated in a fixed-bed reactor. The physico-chemical properties of raw lignites and sorbents were characterized by various techniques. It is found that the sorbents prepared by different lignites exhibited significantly different desulfurization performance due to their different loading contents and utilization rates of active component, and the difference of utilization rates of active component of the sorbents was greater than that of loading contents of active component. The sorbent HPZn/C(Z) prepared by Zhaotong lignite presented the best desulfurization performance owing to its higher content and utilization rate of active component. The loading content of active component depends on pore structure of raw lignite, change of its pore structure high-pressure impregnation process and oxygen-containing functional groups on its surface. The larger pore volume and specific surface area of raw lignite and improvement of its pore volume and specific surface area in high-pressure impregnation process benefit the loading of precursor of active component. Meanwhile, the higher oxygen-containing groups content of raw lignite also favors loading of precursor of active component. The utilization rate of active component is associated with pore structure characteristic of sorbent formed during heat treatment. The combination of S_{total}, V_{total} and $S_{external}/S_{total}$, V_{meso}/V_{total} determine utilization rate of active component. The larger $S_{external}/S_{total}$ and V_{meso}/V_{total} of the sorbent are favorable to effective utilization of active component. Meanwhile, the larger S_{total} and V_{total} of the sorbent are also beneficial to effective utilization of active component when its $S_{external}/S_{total}$ and V_{meso}/V_{total} are larger.

Conflicts of interest

There are no conflicts to declare.

Acknowledgements

The authors gratefully acknowledge the financial support of the Natural Science Foundation of Shanxi Province of China (201701D121122).

References

1 W. Y. Chen and R. N. Xu, *Energy Policy*, 2010, **38**, 2123–2130.
2 D. P. Li, L. Zhang, J. W. Yang, M. X. Lu, J. H. Ding and M. L. Liu, *Int. J. Miner., Metall. Mater.*, 2014, **21**, 388–394.
3 X. Yang, *Renewable Energy*, 2017, **112**, 17–24.
4 W. Torres, S. S. Pansare and J. G. Goodwin Jr, *Catal. Rev.*, 2007, **49**, 407–456.
5 S. Cheah, D. L. Carpenter and K. A. Magrini-Bair, *Energy Fuels*, 2009, **23**, 5291–5307.
6 H. L. Fan, G. J. Shang, L. T. Liang, C. H. Li and J. Y. Lin, *Process Saf. Environ. Prot.*, 2013, **91**, 235–243.
7 H. L. Fan, T. Sun, Y. P. Zhao, G. J. Shang and J. Y. Lin, *Environ. Sci. Technol.*, 2013, **47**, 4859–4865.
8 Y. G. Pan, J. F. Perales, E. Velo and L. Puigjaner, *Fuel*, 2005, **84**, 1105–1109.
9 Z. B. Huang, B. S. Liu, X. Y. Tang, X. Y. Wang and R. Amin, *Fuel*, 2016, **177**, 217–225.
10 Z. F. Zhang, B. S. Liu, F. Wang, W. S. Wang, C. Xia, S. Zheng and R. Amin, *Appl. Surf. Sci.*, 2013, **319**, 961–969.
11 M. M. Wu, L. Shi, T. Lim, A. Vekshab, F. Yu, H. L. Fan and J. Mi, *Chem. Eng. J.*, 2018, **353**, 273–287.
12 Y. C. Park, S. H. Jo, H. J. Ryu, J. H. Moon, C. K. Yi, Y. S. Yoon and J. I. Baek, *Korean J. Chem. Eng.*, 2012, **29**, 1812–1816.
13 S. Y. Jung, S. J. Lee, T. J. Lee, C. K. Ryu and J. C. Kim, *Catal. Today*, 2006, **111**, 217–222.
14 Y. S. Hong, K. R. Sin, J. S. Pak, C. J. Kim and B. S. Liu, *Energy Fuels*, 2017, **31**, 9874–9880.
15 G. Sick and K. Schwerdtfeger, *Metall. Trans. B*, 1987, **18**, 603–609.
16 B. Guo, L. P. Chang and K. C. Xie, *Ind. Eng. Chem. Res.*, 2014, **53**, 8874–8880.
17 Z. F. Zhang, B. S. Liu, F. Wang and J. F. Li, *Energy Fuels*, 2013, **27**, 7754–7761.
18 T. T. Akiti, K. P. Constant, L. K. Doraiswamy and T. D. Wheelock, *Adv. Environ. Res.*, 2001, **5**, 31–38.
19 R. Slimane and J. Abbasian, *Ind. Eng. Chem. Res.*, 2000, **39**, 1338–1344.
20 X. R. Zheng, W. R. Bao, Q. M. Jin, L. P. Chang and K. C. Xie, *Energy Fuels*, 2011, **25**, 2997–3001.
21 M. Ozekmekci, G. Salkic and M. F. Fellah, *Fuel Process. Technol.*, 2015, **139**, 49–60.
22 J. C. Wang, F. L. Ju, L. N. Han, H. C. Qin, Y. F. Hu, L. P. Chang and W. R. Bao, *Energy Fuels*, 2015, **29**, 488–495.

23 F. K. Yin, J. L. Yu, S. Gupta, S. Y. Wang, D. M. Wang, L. Yang and A. Tahmasebi, *Phys. Procedia*, 2012, **24**, 290–296.
24 Q. Liu, Z. F. Zhang, B. S. Liu and H. Xia, *Appl. Catal., B*, 2018, **237**, 855–865.
25 B. Qiu, L. N. Han, J. C. Wang, L. P. Chang and W. R. Bao, *Energy Fuels*, 2011, **25**, 591–595.
26 T. H. Ko, S. M. Wang, F. H. Chang and C. Y. Chu, *RSC Adv.*, 2017, **7**, 35795–35804.
27 T. H. Ko, H. Chu and L. K. Chaung, *Chemosphere*, 2005, **58**, 467–474.
28 Y. R. Dong, X. R. Ren, M. J. Wang, Q. He, L. P. Chang and W. R. Bao, *J. Energy Chem.*, 2013, **22**, 783–789.
29 X. R. Ren, Q. He, Z. Yang, T. Li, L. P. Chang and W. R. Bao, *Process Saf. Environ. Prot.*, 2016, **100**, 142–149.
30 X. R. Ren, Q. He, Y. R. Dong, M. J. Wang, L. P. Chang and W. R. Bao, *Energy Fuels*, 2014, **28**, 4746–4753.
31 Y. L. Zhang, X. X. Jing, K. G. Jing, L. P. Chang and W. R. Bao, *Appl. Surf. Sci.*, 2015, **324**, 90–98.
32 X. B. Xiao, J. P. Cao, X. L. Meng, D. D. Le, L. Y. Li, Y. Ogawa, K. Sato and T. Takarada, *Fuel*, 2013, **103**, 135–140.
33 F. L. Yang, J. P. Cao, X. Y. Zhao, J. Ren, W. Tang, X. Huang, X. B. Feng, M. Zhao, X. Cui and X. Y. Wei, *Energy Convers. Manage.*, 2019, **196**, 1257–1266.
34 T. J. Lee, I. H. Cho and N. K. Park, *Korean J. Chem. Eng.*, 2009, **26**, 582–586.
35 X. R. Zheng, Q. M. Jin, R. Y. He, W. R. Bao and L. P. Chang, *J. China Coal Soc.*, 2011, **36**, 1911–1916.
36 T. H. Ko, H. Chu and L. K. Chaung, *Chemosphere*, 2005, **58**, 467–474.
37 M. Mureddu, I. Ferino, E. Rombi, M. G. Cutrufello, P. Deiana, A. Ardu, A. Musinu, G. Piccaluga and C. Cannas, *Fuel*, 2012, **102**, 691–700.